



Cooperative behavior of molecular motors: Cargo transport and traffic phenomena

Reinhard Lipowsky*, Janina Beeg, Rumiana Dimova, Stefan Klumpp, Melanie J.I. Müller

Theory and Bio-Systems, Max Planck Institute of Colloids and Interfaces, 14424 Potsdam, Germany

ARTICLE INFO

PACS:

87.16.Nn

87.16.Wd

05.40.–a

Keywords:

Molecular motors

Intracellular trafficking

Uni- and bi-directional transport

Traffic jams

Traffic phase transitions

ABSTRACT

All eukaryotic cells including those of our own body contain complex transport systems based on molecular motors which walk along cytoskeletal filaments. These motors are rather small and make discrete mechanical steps with a step size of the order of 10 nm but are able to pull cargo particles over much larger distances, from micrometers up to meters. In vivo, the intracellular cargos include large membrane-bounded organelles, smaller vesicles, a subset of mRNAs, cytoskeletal filaments, and various protein building blocks, which are transported between different cell compartments. This cargo transport is usually performed by teams of motors. If all motors belong to the same molecular species, the cooperative action of the motors leads to uni-directional transport with a strongly increased run length and with a characteristic force dependence of the velocity distributions. If two antagonistic teams of motors pull on the same cargo particle, they perform a stochastic tug-of-war, which is characterized by a subtle force balance between the two motor teams and leads to several distinct patterns of bi-directional transport. So far, all experimental observations on bi-directional transport are consistent with such a tug-of-war. If many motors and/or cargo particles are transported along the filaments, one encounters various traffic phenomena. Depending on their mutual interactions and the compartment geometry, the motors form various spatio-temporal patterns such as traffic jams, and undergo nonequilibrium phase transitions between different patterns of transport.

© 2009 Elsevier B.V. All rights reserved.

1. Introduction

In all living cells including those of our body, we find many different molecular motors and colloidal machines that perform various tasks such as assembly and synthesis of macromolecules, ion transport through membranes, cargo transport along filaments, cell division, and cell locomotion. These motors and machines act as little 'demons' or 'nanorobots' that keep the living cell in a highly ordered state far from equilibrium. This self-organization is based on the energy conversion of the motors, which transform chemical energy, typically arising from ATP hydrolysis, into mechanical work.

Prominent examples for such molecular motors are: (i) DNA and RNA polymerases, which move along the strands of DNA in order to replicate it and to transcribe it into RNA; (ii) ribosomes that attach to mRNA and translate the nucleotide sequence into proteins; (iii) membrane pumps, which transport ions and small molecules across membranes. The resulting concentration gradients may be used in order to drive: (iv) rotary motors such as the bacterial flagellar motor and the F1-ATPase, which are used for

cell locomotion and ATP synthesis, respectively; (v) myosins in muscles, which work in ensembles and collectively displace actin filaments; and (vi) stepping motors, which bind to the filaments of the cytoskeleton and then walk along these filaments in a directed fashion.

In this review, we will focus on this latter class of cytoskeletal motors such as kinesins and dyneins, see Fig. 1(a), that walk processively along cytoskeletal filaments in a directed manner and are essential for intracellular transport, cell division, and cell locomotion [1–3]. Three superfamilies of processive cytoskeletal motors have been identified: kinesins, dyneins, and myosins [3,4]. Kinesins and dyneins bind to microtubules as shown in Fig. 1(a) whereas myosins bind to actin filaments as shown in Fig. 1(b).

The movements of cytoskeletal motors cover many length and timescales [5,6]. Already for a single motor, one can distinguish three dynamical regimes: the single-step dynamics of the motor protein which arises from the coupling of the molecular conformation to ATP hydrolysis; the directed walks of the motor along the filaments; and the composite walks of the motor as it repeatedly unbinds from and rebinds to the filaments.

The single-step regime is governed by the chemomechanical coupling between ATP hydrolysis and spatial displacements and covers all molecular processes up to a single mechanical step of the motor [7]. Kinesin, for example, walks in a 'hand-over-hand' fashion, i.e., by alternating steps, in which one head moves

* Corresponding author.

E-mail address: lipowsky@mpikg.mpg.de (R. Lipowsky).

URL: <http://www.mpihg.mpg.de/th/> (R. Lipowsky).

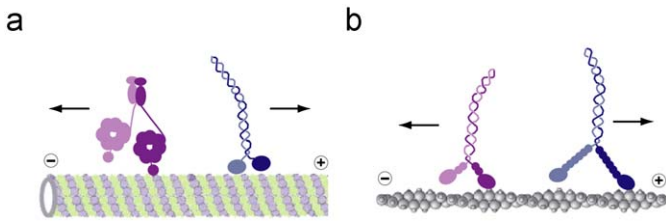


Fig. 1. Stepping motors: (a) microtubule with one dynein (violet) and one kinesin (blue) motor. The filament consists of tubulin dimers that provide a lattice of binding sites with a lattice parameter of 8 nm. (b) Actin filament with one myosin VI (violet) and one myosin V (blue) motor. Both filaments are polar and have two different ends, a plus and a minus end. Each motor walks either towards the plus or the minus end as indicated. (For interpretation of the references to color in this figure legend, the reader is referred to the web version of this article.)

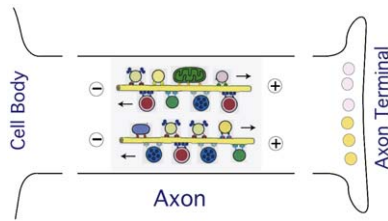


Fig. 2. Two-way traffic in an axon. The traffic is based on microtubules, which provide the tracks, and different types of cytoskeletal motors, which move along these filaments. Each motor species moves either towards the axon terminal (plus direction) or towards the cell body (minus direction). Small teams of motors pull vesicles and other types of cargo over macroscopic distances.

forward by 16 nm while the other one remains bound to the filament [8,9]. During each step, the center-of-mass of the motor is displaced by 8 nm corresponding to the lattice constant of the microtubule. These mechanical steps of kinesin are fast and completed within 15 μ s [10].

Because of thermal noise, the motors can make only a certain number of steps before they detach from the filaments. A single kinesin motor, for example, unbinds from the filament after it has made about a hundred steps, i.e., after a run length (or walking distance) of about 1 μ m [11]. On length scales that are large compared to its run length, a single motor undergoes composite walks consisting of directed (or biased) motion along the filaments interrupted by diffusive (or random) motion in the surrounding solution [12–14].

The run length of single motors is rather small compared to the long distances — centimeters or even meters — over which cargo particles are transported in cells and axons, see Fig. 2. One rather effective way to increase the run length is via cooperative transport of cargo particles by several motor molecules [15]. The corresponding run length distribution has been recently measured for two different *in vitro* assays [16,17].

In vivo, stepping motors are responsible for the intracellular transport of various types of cargo particles such as vesicles, organelles, and filaments. In most cases, this cargo transport is cooperative and performed by several motors as revealed by electron microscopy [18,19] and single particle tracking [20–23]. In some cases, the transport is uni-directional as one would expect if all motors that pull on the cargo belong to the same motor species. In many cases, the cargo moves in a bi-directional manner, which implies that it is pulled by two antagonistic motor teams corresponding to two different motor species.

The experimental observations for bi-directional transport by two motor species are quite complex [24,25]. The cargo may exhibit rather different types of trajectories with and without pauses between forward and backward motion. In addition, changing the molecular structure of one motor species often affects the movement in both directions. Therefore, it was

proposed that this behavior reflects the coordination by an unknown protein complex attached to the cargo. However, we have recently shown that all experimental observations can be explained by a *stochastic tug-of-war* between the two motor species [26,27]. This implies that the signalling pathways for the regulation of intracellular transport may directly target the different motor molecules rather than an additional coordination complex [26,28].

The cartoon in Fig. 2 indicates that the traffic within an axon can be rather dense and, thus, may lead to traffic jams as one would expect theoretically [12,29–31]. There is indeed some experimental evidence for jams of motor particles in axons (W. Saxton, private communication). An extreme case has been induced by mutations of the motor proteins which led to strong swelling of axons [32,33]. Jams of kinesin-like motors have also been found in fungal hyphae as one varied the motor concentration *in vivo* by changing the level of expression of the corresponding gene [34,35]. Recently, motor traffic jams have also been observed in several *in vitro* experiments [36–39]. Apart from crowding and traffic jams, the mutual interaction between motors and filaments leads to *nonequilibrium phase transitions* as has been shown theoretically both for stepping motors on immobilized filaments [29,40,30] and for gliding filaments on immobilized motors [41,42].

This review is organized as follows. First, we briefly review the properties of single motors in Section 2. We then discuss uni-directional transport of a single cargo particle by one team of N identical motors, see Section 3. Compared to the behavior of a single motor, such a cargo particle exhibits a run length that increases strongly with N and an apparent stall force that increases sublinearly with N . In Section 4, bi-directional transport of a single cargo particle is considered, in which this particle is pulled by two teams of plus and minus motors. The two motor teams perform a stochastic tug-of-war that is characterized by strongly fluctuating forces acting on each motor arising from the force balance between the two teams. As a result, one finds several distinct motility regimes, which are determined by the numbers N_+ and N_- of plus and minus motors as well as by the single motor parameters. All available experimental data on bi-directional cargo transport can be understood in terms of such a tug-of-war. Finally, the traffic of interacting motors and cargo particles is briefly discussed in Section 5. Depending on their interactions and the compartment geometry, the motors form various spatio-temporal patterns such as traffic jams and undergo nonequilibrium phase transitions between different patterns of transport.

2. Properties of single motors

Since we are interested in the movements of molecular motors on length scales that exceed the run length of a single motor, we focus on those motor properties that are relevant on these scales. We neglect the details of the protein structure and stepping cycle [43–45] of the motor and describe their behavior in terms of the following six parameters that govern their stepping, unbinding, and rebinding.

First, the average velocity of the bound motor has the value v_f in the absence of load, vanishes at the stall force $F = F_s$, and is characterized by the velocity scale v_b with $v_b \ll v_f$ for $F > F_s$. Second, the unbinding of the motor from the filament is governed by the unbinding rate ω_{off} which can be parametrized by the zero-force unbinding rate κ_{off} and the detachment force F_d . Finally, the binding or rebinding of the motor to the filament is described by the motors' binding rate ω_{on} , which increases with the local motor

concentration. These different parameters will now be explained in more detail.

2.1. Average velocity of stepping motors

A single motor that is bound to a filament steps along this filament with a certain average velocity v which depends, in general, on the load force and on the nucleotide concentrations. As one increases the load force F , the velocity decreases, vanishes at the stall force $F = F_s$, and becomes negative for superstall forces. This relationship between velocity and force can be written in the general form

$$v = \mathcal{V}(F) \quad \text{with} \quad \mathcal{V}(F = F_s) = 0, \quad (2.1)$$

where $\mathcal{V}(F)$ is a monotonically decreasing function of F . A convenient parametrization of the function \mathcal{V} is provided by

$$\mathcal{V}(F) = v_f(1 - F/F_s) \quad \text{for} \quad 0 \leq F \leq F_s, \quad (2.2)$$

with the forward velocity $v_f = \mathcal{V}(F = 0)$ and [26]

$$\mathcal{V}(F) = v_b(1 - F/F_s) \quad \text{for} \quad F_s \leq F, \quad (2.3)$$

with the backward velocity scale $v_b \ll v_f$. Thus, the stall force F_s may be regarded as the largest force that the motor can generate.

For conventional kinesin (or kinesin-1), the stall force F_s was measured by several groups: Visscher et al. [46] found this force to vary between 5.5 and 7 pN depending on the ATP concentration whereas Nishiyama et al. [47] and Carter and Cross [10] found the ATP-independent values 7.6 and 7 pN, respectively. The zero-force velocity v_f is of the order of $1 \mu\text{m/s}$ [46,47,10], and the backward velocity scale v_b is about 6 nm/s [47,10].

2.2. Run length and unbinding rate

Because of thermal noise, a single motor must eventually unbind from the filament. Thus, a single motor can be characterized by its average run or binding time $\langle \Delta t \rangle$ and the corresponding unbinding rate

$$\omega_{\text{off}} \equiv 1/\langle \Delta t \rangle. \quad (2.4)$$

During its run time, the single motor steps along the filament and covers the average run length

$$\langle \Delta x \rangle = v \langle \Delta t \rangle. \quad (2.5)$$

In the absence of load, kinesin motors bound to microtubules make about a 100 successive steps [11] which corresponds to an average run length $\langle \Delta x \rangle \simeq 1 \mu\text{m}$ and an average run time $\langle \Delta t \rangle \simeq 1 \text{ s}$. In the absence and presence of dynactin, an accessory protein, dynein motors make about 20 and 40 successive steps, respectively [48]. Myosin V, which moves along actin filaments, makes about 50 steps before it unbinds again corresponding to a run length of about $1.5 \mu\text{m}$ [49]. Myosin VI, on the other hand, makes only about nine successive steps, i.e., its average run length is about 280 nm [50].

The unbinding of a single motor is an activated process governed by a corresponding energy barrier. In the presence of an external force F that acts to detach the motor, this barrier is reduced by $F\ell_d$ where ℓ_d represents an appropriate molecular length scale, which characterizes the elastic deformation of the motor molecule required for its detachment. Therefore, the unbinding rate ω_{off} is expected to have the general form [15]

$$\omega_{\text{off}}(F) = \kappa_{\text{off}} \exp(\ell_d F/k_B T) \equiv \kappa_{\text{off}} \exp(F/F_d) \quad (2.6)$$

as follows from Kramers theory [51] for activated processes with the zero-force unbinding rate κ_{off} and the detachment force

$$F_d \equiv k_B T/\ell_d. \quad (2.7)$$

Such a force dependence of the unbinding rate has been obtained from an exponential fit to the experimental data in Ref. [52] and from a detailed network representation of the kinesin motor [43,7].

2.3. Binding rate

An unbound motor that diffuses in the surrounding medium and comes close to a filament can bind to this filament. This rebinding was first described in terms of sticking (or binding) probabilities for discrete-time motor walks [12,13]. The corresponding binding rate ω_{on} , which is equal to the number of motors that bind to a single filament site per unit time, depends on the local concentration of the unbound motors. When the motors can diffuse far away from the filaments within an extended compartment, this concentration corresponds to the molar concentration C . If the unbound motors are kept in the vicinity of the filaments, e.g., by being attached to cargo particles that move along the filaments, this concentration should be regarded as an effective concentration C_{eff} , see Eq. (3.6) below.

In order to estimate the binding rate for filaments in contact with a reservoir of freely diffusing motors, let us consider a system with volume V that contains a certain number of filament binding sites N_{si} as well as a certain number of motors $N_{\text{mo}} = N_{\text{b}} + N_{\text{ub}}$ where N_{b} and N_{ub} represent the average number of bound and unbound motors, respectively. We then obtain the molar concentration

$$C \equiv N_{\text{ub}}/N_{\text{Av}}V \quad (2.8)$$

of the motors with Avogadro's number $N_{\text{Av}} \simeq 6 \times 10^{23}$ (assuming that the filament volume can be neglected) and the binding ratio

$$n_{\text{b}} \equiv N_{\text{b}}/N_{\text{si}}. \quad (2.9)$$

The dissociation constant C_{dis} is then defined by the relation

$$n_{\text{b}} \approx C/C_{\text{dis}} \quad \text{for small } C. \quad (2.10)$$

For molar concentrations $C \gtrsim C_{\text{dis}}$, the binding ratio $n_{\text{b}} \lesssim 1$ and the binding sites of the filaments are more or less covered by motors. For kinesin, e.g., the dissociation constant $C_{\text{dis}} \simeq 100 \text{ nM}$ for typical in vitro assays. This molar concentration corresponds to an average motor-motor separation of about 255 nm within such an assay. This implies that the filaments become already overcrowded with kinesin motors for a rather dilute bulk concentration of the motors.

The dependence of the binding rate ω_{on} on the molar concentration C is now described by

$$\omega_{\text{on}} \approx \kappa_{\text{on}} C \quad \text{for small } C, \quad (2.11)$$

which defines the binding rate constant κ_{on} . In the steady state, the binding flux ω_{on} must balance the unbinding flux $\omega_{\text{off}} n_{\text{b}}$. Using the asymptotic relations (2.11) and (2.10), this flux balance equation becomes

$$\omega_{\text{on}} \approx \kappa_{\text{on}} C \approx \omega_{\text{off}} n_{\text{b}} \approx \omega_{\text{off}} C/C_{\text{dis}} \quad (2.12)$$

for small C which implies that the binding rate constant κ_{on} satisfies the relation

$$\kappa_{\text{on}} = \frac{\omega_{\text{off}}}{C_{\text{dis}}} = \frac{1}{\langle \Delta t \rangle C_{\text{dis}}}. \quad (2.13)$$

3. Uni-directional transport by one motor team

Now, consider a single cargo particle with N motors, which are firmly attached to this particle, see Fig. 3. Each of these motors can

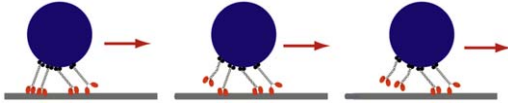


Fig. 3. Uni-directional transport of a cargo particle by $N = 4$ identical motors. The motors are firmly attached to the particle but unbind from and rebind to the filament. Therefore, the actual number n of pulling motors varies with time between $n = 0$ and N .

act as a crosslinker between the cargo and the filament and, thus, actively pull on the cargo. However, because of the finite run length and run time of the motors, the actual number n of pulling motors is not constant but varies with time between zero and N . Thus, if we include the unbound state with $n = 0$, the cargo can be in $N + 1$ different states (n), which are distinguished by the number n of active pulling motors.

If the cargo is in state (n), the binding of one motor to the filament leads to state ($n + 1$) and the unbinding of one motor from the filament to state ($n - 1$). The transition from state (n) to state ($n + 1$) with binding rate $\omega_{n,n+1}$, the transition from (n) to ($n - 1$) with unbinding rate $\omega_{n,n-1}$, the transition from (n) to ($n + 1$) with binding rate $\omega_{n,n+1}$. The probabilities $P_n = P_n(t)$ that the cargo particle is in state (n) at time t then evolve according to the master equation [15]

$$\frac{\partial}{\partial t} P_n = -\Delta J_{n,n+1} - \Delta J_{n,n-1}, \quad (3.1)$$

with

$$\Delta J_{n,n+1} \equiv P_n \omega_{n,n+1} - P_{n+1} \omega_{n+1,n} \quad (3.2)$$

and

$$\Delta J_{n,n-1} \equiv P_n \omega_{n,n-1} - P_{n-1} \omega_{n-1,n}. \quad (3.3)$$

In the steady state, the probability distribution $P_n = P_n^{\text{st}}$ satisfies

$$P_{n+1}^{\text{st}} \omega_{n+1,n} = P_n^{\text{st}} \omega_{n,n+1} \quad (3.4)$$

for $0 \leq n \leq N - 1$. This relation corresponds to detailed balance between the states ($n + 1$) and (n) and reflects the fact that all movements of the bound cargo particle begin and end with $n = 0$ and that every transition from (n) to ($n + 1$) implies a backward transition at some later time. It is also implicitly assumed here that the binding and unbinding rates are independent of the transition rates for stepping along the filament.

In vivo, the pulling motors are attached to their cargo via a long and flexible stalk. In addition, electron micrographs indicate that the spacing of the motors on the cargo is comparable to their length. We now focus on such a ‘dilute’ regime, in which the motors do not interfere with each other apart from the fact that they are attached to the same cargo. In this case, the transition rates $\omega_{n,n-1}$ and $\omega_{n,n+1}$, have the simple form [15]

$$\omega_{n,n-1} = n \omega_{\text{off}} \quad \text{and} \quad \omega_{n,n+1} = (N - n) \omega_{\text{on}}, \quad (3.5)$$

where the combinatorial factors n and $N - n$ arise from the different possibilities to unbind or bind a motor when the cargo particle is in state (n). The unbinding rate ω_{off} is taken to be equal to the unbinding of a *single* motor as given by Eq. (2.4).¹ The binding rate ω_{on} , on the other hand, reflects the effective motor concentration, C_{eff} , between the cargo particle and the filament. Thus, the binding rate of a single motor attached to the cargo should have the form

¹ Strictly speaking, the unbinding motor heads always experience some constraints arising from the attachment of the other end of the motor to the cargo particle. These constraints are ignored here.

$$\omega_{\text{on}} = \kappa_{\text{on}} C_{\text{eff}}. \quad (3.6)$$

As mentioned, kinesin is characterized by the unbinding rate $\omega_{\text{off}} \approx 1/\text{s}$ and the binding rate constant $\kappa_{\text{on}} \approx 10/(\mu\text{M s})$. In Ref. [15], we used the estimate $\omega_{\text{on}} = 5/\text{s}$ for kinesin as suggested by experiments in which the motors pull membrane tubes [37]. This value for the binding rate ω_{on} corresponds to an effective molar concentration $C_{\text{eff}} \approx 0.5 \mu\text{M}$ or an average separation between the motors of about 150 nm.

3.1. Regime of low load force

As emphasized before, the number of pulling motors changes with time in a stochastic manner. It is then instructive to consider the average number $\langle n \rangle$ of pulling motors where the average is taken over all bound states of the motor. If the cargo particle does not experience a load force or, more generally, if this load force is sufficiently small, this average number can be calculated explicitly for noninterfering motors. If the cargo particle is initially bound to the filament by a single motor, i.e., $n(t = 0) = 1$, one obtains the expression [15]

$$\langle n \rangle = \frac{1}{1 + k_{\text{off}}} \frac{(1 + k_{\text{off}})^N}{(1 + k_{\text{off}})^N - k_{\text{off}}^N} N \leq N, \quad (3.7)$$

which depends on the maximal motor number N and on the dimensionless desorption coefficient for zero force as given by

$$k_{\text{off}} \equiv \omega_{\text{off}}(F = 0)/\omega_{\text{on}} = \omega_{\text{off}}/\kappa_{\text{on}} C_{\text{eff}} = C_{\text{dis}}/C_{\text{eff}}, \quad (3.8)$$

with the motor’s dissociation constant C_{dis} as defined in Eq. (2.10). Since the average in Eq. (3.7) is taken over the bound states of the cargo particle, one has $1 \leq \langle n \rangle \leq N$; the limiting values $\langle n \rangle = 1$ and $\langle n \rangle = N$ are attained for large and small k_{off} , respectively. Furthermore, the relation (3.7) leads to $\langle n \rangle \approx N/(1 + k_{\text{off}})$ for large N .

When the noninterfering motors pull on the cargo in the absence of load, they move with their single motor velocity v . Thus, in this situation, the cargo particle also has velocity $v_{\text{ca}} = v$ for all cargo states (n). The average run length $\langle \Delta x_{\text{ca}} \rangle$ of the cargo particle is then given by [15]

$$\langle \Delta x_{\text{ca}} \rangle \approx (v/\omega_{\text{off}} N)(1/k_{\text{off}})^{N-1} \quad (3.9)$$

and the corresponding unbinding rate by

$$\omega_{\text{off,ca}} = v/\langle \Delta x_{\text{ca}} \rangle \approx \omega_{\text{off}} N k_{\text{off}}^{N-1} \quad (3.10)$$

for small zero-force desorption coefficient $k_{\text{off}} = \omega_{\text{off}}/\omega_{\text{on}} \ll 1$, i.e., for strongly binding motors. Thus, in this case, the run length increases exponentially and the unbinding rate decreases exponentially with increasing number of motors. It is interesting to note that the two relations (3.9) and (3.10) are also valid for a cargo particle with $N = 1$ and then reduce to $\langle \Delta x_{\text{ca}} \rangle = \langle \Delta x \rangle$ and $\omega_{\text{off,ca}} = \omega_{\text{off}}$. If the cargo is pulled by up to N kinesin motors with $k_{\text{off}} \approx 0.2$, the expression as given by Eq. (3.9) leads to the estimate $\langle \Delta x_{\text{ca}} \rangle \approx 5^{N-1}/N \mu\text{m}$ which implies that $N = 7$ or 8 kinesin molecules are sufficient to attain an average run length in the centimeter range.

3.2. Run length distributions

In addition to the average value $\langle \Delta x_{\text{ca}} \rangle$ of the run length, the model described in the previous subsection can also be used to calculate the full run length distribution $\Psi(\Delta x_{\text{ca}})$ [15], which develops a ‘fat’ tail for $N > 1$ as shown in Fig. 4. In this figure, the theoretical distributions are compared with experimental ones that have been obtained in vitro by preparing carboxylated polystyrene beads covered with kinesin [17]. In order to vary the

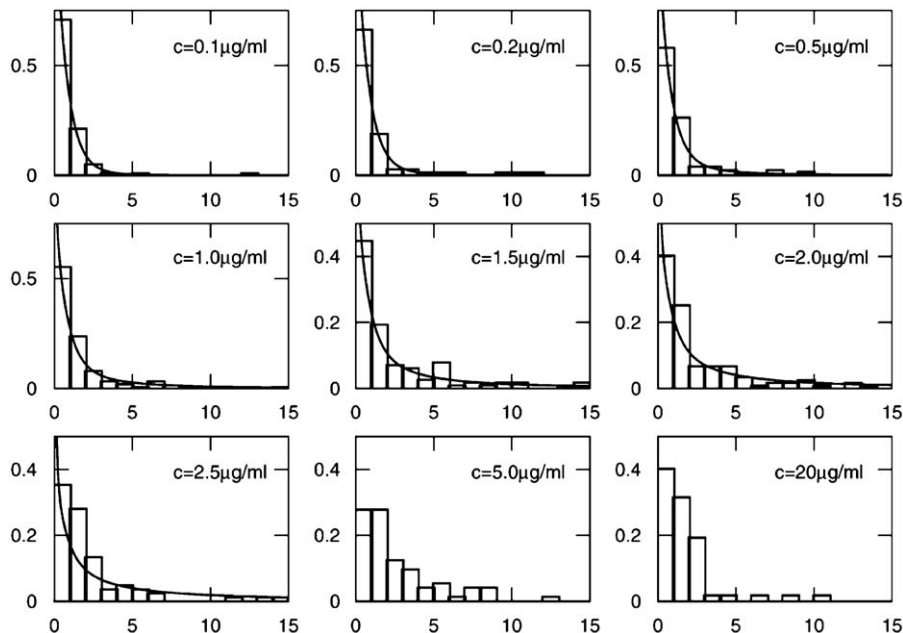


Fig. 4. Run length distributions $\Psi(\Delta x_{ca})$ of cargo particles that have been incubated at different mass densities c of kinesin. In each panel, the columns represent the experimental data, and the full lines the theoretical curves as obtained from Eq. (3.17). The seven curves for the mass densities $0.1 \mu\text{g/ml} \leq c \leq 2.5 \mu\text{g/ml}$ have been obtained using the density scale $c_0 = 0.79 \mu\text{g/ml}$ and the binding rate $\omega_{on} = 5.1/\text{s}$. This implies that the average number $\langle n \rangle$ of pulling motors increases from $\langle n \rangle = 1.1$ for $c = 0.1 \mu\text{g/ml}$ to $\langle n \rangle = 3.2$ for $c = 2.5 \mu\text{g/ml}$. For concentrations c that are comparable to or larger than $5 \mu\text{g/ml}$, the linear relation (3.12) between $\langle N \rangle$ and c is no longer fulfilled [17].

motor coverage of the beads, the mass density c of the kinesin molecules in the incubation chamber is changed for fixed bead concentration. The coverage increases linearly over a certain mass density range until saturation is reached as deduced from dynamic light scattering experiments. The maximal coverage is estimated to be about 130 motors per bead.

When a bead prepared in this way is brought into contact with immobilized microtubules, only a relatively small fraction of the attached motors can pull simultaneously on the bead. The maximal number of motors that can do so corresponds to the number N as defined for a single cargo particle in the previous subsection. Because of the used preparation method, this number varies from bead to bead. Thus, if one observes a large number \mathcal{N}_{bea} of different beads, the behavior of this ensemble of cargo particles involves the additional distribution $P_{\text{bea}}(N)$ for the number N . The simplest choice for $P_{\text{bea}}(N)$ is a Poisson distribution

$$\mathcal{P}_{\text{Po}}(N) \equiv \frac{(c/c_0)^N e^{-c/c_0}}{N!}, \quad (3.11)$$

which leads to the average number

$$\langle N \rangle = c/c_0, \quad (3.12)$$

where the density scale c_0 is used as a fit parameter and obtained from the detailed comparison between theory and experiment, see Fig. 4. Since the average number $\langle N \rangle$ turns out to be relatively small, it is convenient to use the truncated Poisson distribution as given by [17]

$$P_{\text{bea}}(N) = \frac{1}{Z} \mathcal{P}_{\text{Po}}(N) \quad \text{for } 1 \leq N \leq N_{\text{max}}, \quad (3.13)$$

with the normalization constant

$$Z \equiv \sum_{N=1}^{N_{\text{max}}} \mathcal{P}_{\text{Po}}(N). \quad (3.14)$$

The maximal number N_{max} is chosen in such a way that all \mathcal{N}_{bea} beads, for which the run length is determined in the experiments, are likely to have $N \leq N_{\text{max}}$ motors attached to them. This

condition can be ensured by

$$\mathcal{N}_{\text{bea}} \frac{\mathcal{P}_{\text{Po}}(N_{\text{max}})}{(1 - \mathcal{P}_{\text{Po}}(0))} \geq 1 \quad (3.15)$$

and

$$\mathcal{N}_{\text{bea}} \frac{\mathcal{P}_{\text{Po}}(N_{\text{max}} + 1)}{(1 - \mathcal{P}_{\text{Po}}(0))} < 1. \quad (3.16)$$

The theoretical run length distributions $\Psi(\Delta x_{ca})$ as shown in Fig. 4 have been obtained by first calculating the run length distributions $\Psi_N(\Delta x_{ca})$ for each $N \leq N_{\text{max}}$ and then taking the average over N which leads to

$$\Psi(\Delta x_{ca}) = \sum_{N=1}^{N_{\text{max}}} P_{\text{bea}}(N) \Psi_N(\Delta x_{ca}). \quad (3.17)$$

These theoretical distributions were fitted to seven experimental distributions using only two fit parameters, namely the density scale c_0 and the binding rate ω_{on} . The best fit was obtained for $c_0 = 0.79 \mu\text{g/ml}$ and $\omega_{on} = 5.1/\text{s}$, see Fig. 4.

As a result, the maximal motor number N_{max} is found to vary between $N_{\text{max}} = 2$ and 7 for mass densities c between 0.1 and $2.5 \mu\text{g/ml}$ corresponding to molar concentrations between 0.27 and 6.7 nM . In the same concentration range, the average number $\langle n \rangle$ of pulling motors is found to lie between $\langle n \rangle = 1.1$ and 3.2 motors.

All distributions $\Psi(\Delta x_{ca})$ in Fig. 4 decrease monotonically with increasing run length Δx_{ca} . Such a monotonic decay is expected since these run length distributions were obtained for beads that bind after diffusing towards the filaments. Indeed, such a deposition method implies that the beads are initially connected to the filaments by a single motor molecule corresponding to the initial condition $P_n(t=0) = \delta_{n,1}$ [15,17]. Recently, a somewhat different run length distribution has been reported in Ref. [16]. This latter run length distribution was obtained by grouping all runs that exceeded $8 \mu\text{m}$ into a single bin. Furthermore, the deposition of the kinesin-coated beads onto the microtubules was

performed by optical tweezers. In the concentration regime, in which such a bead carries several motors, this deposition method is likely to lead to an initial state of the bound bead, in which this bead is connected to the microtubule by several motors. In such a situation, the run length distribution can develop a maximum which is expected to lie below 1 μm .

A more direct comparison between theory and experiment would be possible if one prepared cargo particles with a precise number $N > 1$ of motors attached to each of them. One appealing approach consists in crosslinker molecules, each of which binds $N > 1$ motors. One could then study the attachment of these crosslinkers in the dilute limit, in which the cargo particle carries at most one crosslinker. So far, such a preparation method has not been developed.

3.3. Force dependence of uni-directional transport

If the cargo particle does not experience a load force, noninterfering motors unbind and rebind in a statistically independent manner. In contrast, in the presence of such a force, even noninterfering motors become coupled via the cargo. If the cargo is subject to the force F , the n active motors share this force, and each single motor feels the reduced force

$$F_1 \equiv F/n, \quad (3.18)$$

which now depends on n . Since n changes with time in a stochastic manner, so does the force F_1 acting on each motor. In order to understand the consequence of this coupling between the motors, one has to take the force dependence of the different transition rates into account.

The unbinding rate ω_{off} of a single motor increases exponentially with the load force F , see Eq. (2.6). Thus, a single motor that experiences the load force $F_1 = F/n$ unbinds from the filament with unbinding rate $\omega_{\text{off}} = \kappa_{\text{off}} \exp(F/nF_d)$ where F_d denotes the detachment force of a single motor as before. It then follows from Eq. (3.5) that the transition rate from cargo state (n) to state ($n-1$) is given by

$$\omega_{n,n-1} \equiv \omega_{\text{off}}(n) = n\kappa_{\text{off}} e^{F_1/F_d} = n\kappa_{\text{off}} e^{F/nF_d}. \quad (3.19)$$

Thus, all unbinding rates increase exponentially with increasing load and the corresponding force scale nF_d depends on the number n of pulling motors.

As long as the cargo particle is bound to the filament, i.e., for $n \geq 1$, the effective motor concentration C_{eff} between the cargo and the filament, which enters the binding rate ω_{on} of a single motor attached to the cargo, see Eq. (3.6), cannot be substantially reduced by the load force F . The simplest assumption that is consistent with this constraint is to consider the force-independent binding rate

$$\omega_{n,n+1} \equiv \omega_{\text{on}}(n) = (N-n)\kappa_{\text{on}} C_{\text{eff}}(F=0) = (N-n)\omega_{\text{on}}, \quad (3.20)$$

compare Eq. (3.6).

For noninterfering motors as considered here, the steady state probabilities P_n^{st} to find the cargo particle in state (n) are now given by the explicit expression

$$P_n^{\text{st}} = \bar{P}_n^{\text{st}} / \Omega \quad \text{with} \quad \Omega \equiv \sum_{n=0}^N \bar{P}_n^{\text{st}} \quad (3.21)$$

and the unnormalized probabilities

$$\begin{aligned} \bar{P}_n^{\text{st}} &= 1 \quad \text{for} \quad n=0 \\ &= \binom{N}{n} \left(\frac{1}{k_{\text{off}}} \right)^n e^{-H_n F/F_d} \quad \text{for} \quad n \geq 1, \end{aligned} \quad (3.22)$$

which depend on the binomial coefficient $\binom{N}{n}$, the zero-force desorption coefficient k_{off} as in Eq. (3.8), and the harmonic numbers

$$H_n \equiv \sum_{m=1}^n \frac{1}{m} \quad (3.23)$$

as follows from Eq. (3.4).²

Since $H_1 = 1$ and $H_{n+1} > H_n$, the normalization factor Ω in Eq. (3.21) has the asymptotic behavior

$$\Omega \approx 1 + \frac{N}{k_{\text{off}}} e^{-F/F_d} \quad \text{for} \quad F \gg F_d. \quad (3.24)$$

Furthermore, since the harmonic numbers H_n satisfy the inequalities $c_{\text{Eu}} + \ln(n) < H_n \leq 1 + \ln(n)$ with Euler's constant $c_{\text{Eu}} \approx 0.577$, the exponential factors of the unnormalized probabilities \bar{P}_n^{st} as given by Eq. (3.22) satisfy the inequalities

$$\frac{e^{-c_{\text{Eu}} F/F_d}}{n^{F/F_d}} \leq e^{-H_n F/F_d} \leq \frac{e^{-F/F_d}}{n^{F/F_d}}. \quad (3.25)$$

Because the noninterfering motors interact only via their common cargo, the steady state probabilities P^{st} depend only on the detachment force F_d but not on the stall force F_s , which characterizes the force-velocity relationship (2.1) of a single motor. Since the force acting on the cargo particle is shared by the n pulling motors, they all experience, on average, the same force $F_1 = F/n$ and, thus, have the same velocity equal to the instantaneous cargo velocity

$$v_{\text{ca},n}(F) = \mathcal{V}(F/n) = \mathcal{V}(F_1). \quad (3.26)$$

As a pulling motor unbinds from the filament, the force acting on a single motor increases from $F_1 = F/n$ to $F/(n-1)$ and the instantaneous cargo velocity decreases from $\mathcal{V}(F/n)$ to $\mathcal{V}(F/(n-1))$. Likewise, as a detached motor rebinds to the filament, the instantaneous velocity increases from $\mathcal{V}(F/n)$ to $\mathcal{V}(F/(n+1))$. In the steady state, the average cargo velocity v_{ca} is then given by

$$v_{\text{ca}}(F) = \sum_{n=1}^N P_n^{\text{st}} v_{\text{ca},n}(F) = \sum_{n=1}^N \binom{N}{n} \left(\frac{1}{k_{\text{off}}} \right)^n \Psi_n(F), \quad (3.27)$$

with the force-dependent factors

$$\Psi_n(F) \equiv \frac{1}{\Omega} \exp[-H_n F/F_d] \mathcal{V}(F/n). \quad (3.28)$$

With increasing load force F , the normalization factor $\Omega \approx 1$ as in Eq. (3.24), and the force dependence of $\Psi_n(F)$ is governed (i) by the exponential factor $\exp[-H_n F/F_d]$ which decreases monotonically with increasing F as follows from Eq. (3.25) and (ii) by the instantaneous velocity $\mathcal{V}(F/n)$, which also decreases monotonically and vanishes for $F = nF_s$ with the stall force F_s of a single motor.

For $n \leq F/F_s$, the instantaneous velocity $\mathcal{V}(F/n)$ is governed by backward steps and, thus, rather small.³ Thus, for $F > mF_s$, only cargo states (n) with $n > m$ contribute significantly to the sum in Eq. (3.27), and their contribution is reduced by the factor $1/n^{F/F_d} < 1/m^{F/F_d}$. As a result, the cargo velocity seems to vanish at an apparent stall force $\hat{F}_{s,N}$, which is smaller than the true stall $F_{s,N} \equiv NF_s$. For kinesin with $k_{\text{off}} = 0.2$ and $F_s = 6$ pN, for example,

² In general, the probability P_0^{st} for the unbound state of the cargo is $P_0^{\text{st}} = 1/\Omega$ with the normalization factor Ω as in (3.21). For $F=0$, one has $P_0^{\text{st}} = 1/(1 + \omega_{\text{on}}/\omega_{\text{off}})^N$.

³ In general, the terms with $n < F/F_s$ give a small and negative contribution to the sum in Eq. (3.27).

one finds $\hat{F}_{s,5} \simeq 20$ pN and $F_{s,5} = 30$ pN as well as $\hat{F}_{s,10} \simeq 30$ pN and $F_{s,10} = 60$ pN [15]. Thus, the apparent stall force $\hat{F}_{s,N}$, which may be viewed as the force generated by the team of N motors, increases with N but is substantially smaller than $F_{s,N} = NF_s$ for large N .

In Ref. [15], both the average cargo velocity $v_{ca}(F)$ and the probability distribution for the instantaneous velocity of the cargo have been calculated for kinesin with $k_{off} \simeq 0.2$. With increasing load, the latter distribution is shifted towards smaller velocity values, becomes broader, and develops several peaks in agreement with recent experimental observations on the in vivo transport of vesicles and organelles [21,23]. Velocity distributions with multiple peaks have also been measured in Ref. [22] but the latter distributions presumably reflect a combination of motor transport, microtubule bending, and the algorithm used for data analysis.

4. Bi-directional transport by two motor teams

In biological cells, the motion of cargo particles along microtubules is often observed to be bi-directional in the sense that the particle frequently switches its direction of motion. Since both kinesin and dynein motors are bound to these particles, it is rather natural to assume that the bi-directional motion arises from the competition between these two motor species. The molecular mechanism underlying this competition has been controversial for some time.

Two scenarios have been discussed [24,25]: (i) tug-of-war between two motor teams: Each motor species tries to move the cargo into its own direction, thereby performing a tug-of-war on the cargo as illustrated in Fig. 5. (ii) Coordination by a putative protein complex: Such a complex could prevent opposing motors from being active at the same time, thereby excluding state (0) in Fig. 5. The observed complexity of bidirectional transport has led many authors to reject a tug-of-war scenario and to search for a coordination complex. However, as recently shown in Ref. [26], this conclusion was premature because the stochastic nature of a realistic tug-of-war leads to rather complex transport behavior as observed experimentally.

Thus, let us consider a team of plus and a team of minus motors that pull in opposite directions; the direction of instantaneous motion is determined by the stronger team as in the two states (+) and (−) of Fig. 5. However, since the number of motors that actually pull varies with time in a stochastic manner for both motor species, the weaker team may suddenly become the stronger one which reverses the direction of motion. Indeed, because of the stochastic unbinding and rebinding of the motors, each individual motor experiences a strongly fluctuating load force. The instantaneous value of this force depends both on the number of motors that pull in the opposite direction and on the number of motors that pull in the same direction since the latter number determines how many motors share the force generated by the opposing team.

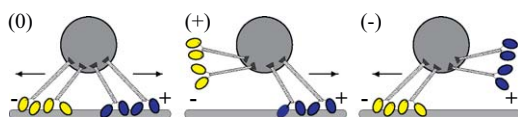


Fig. 5. Cargo transport by 2 plus (blue) and 2 minus (yellow) motors: possible configurations (0), (+), and (−) of motors bound to the microtubule. For configuration (0), the motors block each other so that the cargo does not move. For configuration (+) and (−), the cargo exhibits fast plus and minus motion, respectively [26]. (For interpretation of the references to color in this figure legend, the reader is referred to the web version of this article.)

4.1. Single motor properties and sign conventions

In order to describe the movements of both motor species in a consistent manner, we have to be careful about the signs of their velocities and the signs of the forces experienced by them. We will use the conventions (i) that the velocity of a plus motor is positive in the absence of force, which implies that the zero-force velocity of a minus motor is negative, and (ii) that a load force F is positive if it acts against the forward direction of the plus motors which is identical to the backward direction of the minus motors. Both conventions have also been used in the previous sections for the plus motor kinesin. In addition, we will also take the detachment and stall forces of both motor species to be positive.

Each motor species is now characterized by (i) its force-velocity relationship, which has the general form (2.1) and will be parametrized as in Eqs. (2.2) and (2.3), (ii) its force-dependent unbinding rate ω_{off} , which defines the detachment force F_d as in Eqs. (2.6) and (2.7), and (iii) its binding rate constant κ_{on} as in Eqs. (2.11) and (3.6).

Plus motors. The force-velocity relationship of the plus motors is now given by

$$\begin{aligned} v_+ &= \mathcal{V}_+(F_{1+}) > 0 \quad \text{for } F_{1+} < F_{s,+} \\ &= \mathcal{V}_+(F_{1+}) < 0 \quad \text{for } F_{1+} > F_{s,+}, \end{aligned}$$

with their stall force $F_{s,+}$ defined by

$$\mathcal{V}_+(F_{1+} = F_{s,+}) = 0. \quad (4.1)$$

Furthermore, if a single *plus* motor feels the load force $F = F_{1+} > 0$, its unbinding rate is given by

$$\omega_{off,+} = \kappa_{off,+} e^{F_{1+}/F_{d,+}}, \quad (4.2)$$

which depends on the detachment force $F_{d,+}$ of this motor. The binding rate of each plus motor is taken to be

$$\omega_{on,+} = \kappa_{on,+} C_{+,eff}, \quad (4.3)$$

where $C_{+,eff}$ denotes the effective molar concentration of the plus motors between the cargo particle and the filament, again assumed to be independent of load force.

Minus motors. The minus motors are characterized by the force-velocity relationship

$$\begin{aligned} v_- &= \mathcal{V}_-(|F_{1-}|) < 0 \quad \text{for } |F_{1-}| < F_{s,-} \\ &= \mathcal{V}_-(|F_{1-}|) > 0 \quad \text{for } |F_{1-}| > F_{s,-} \end{aligned}$$

and the implicit equation

$$\mathcal{V}_-(|F_{1-}| = F_{s,-}) = 0 \quad (4.4)$$

for the stall force $F_{s,-}$.

If the *minus* motors feel a load force $F = F_{1-} < 0$, they are governed by the unbinding rate

$$\omega_{off,-} = \kappa_{off,-} e^{|F_{1-}|/F_{d,-}}, \quad (4.5)$$

which involves the corresponding detachment force $F_{d,-}$. The binding rate of a single minus motor is also taken to be force-independent and given by

$$\omega_{on,-} = \kappa_{on,-} C_{-,eff}, \quad (4.6)$$

with the effective concentration $C_{-,eff}$ of minus motors between the cargo particle and the filament.

As emphasized in Section 2, almost all of these single motor parameters can be determined from a systematic analysis of experimental data. For the plus motor kinesin, for example, the zero-force unbinding rate $\kappa_{off,+} \simeq 1/s$, the detachment force $F_{d,+} \simeq 3-5$ pN, the binding rate constant $\kappa_{on,+} \simeq 10/(\mu Ms)$, and the stall force $F_{s,+} \simeq 6-7$ pN as mentioned before. The only

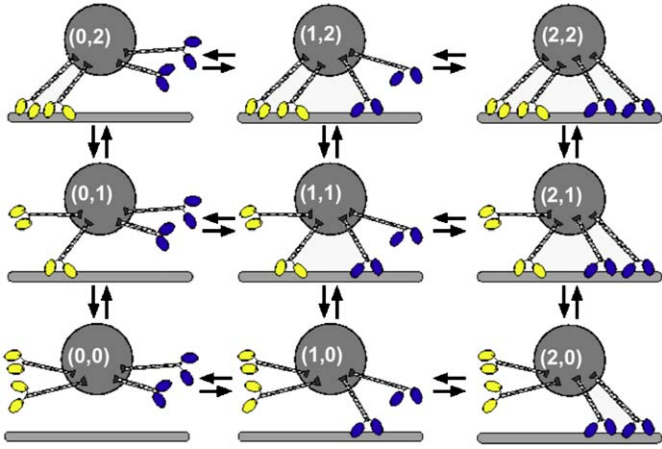


Fig. 6. State space of cargo with $N_+ = 2$ plus and $N_- = 2$ minus motors. The $(N_+ + 1)(N_- + 1)$ states are labeled by (n_+, n_-) corresponding to n_+ plus (blue) and n_- minus (yellow) motors, that simultaneously pull on the cargo. These states form a square lattice with $0 \leq n_+ \leq N_+$ and $0 \leq n_- \leq N_-$. (For interpretation of the references to color in this figure legend, the reader is referred to the web version of this article.)

quantities that are difficult to measure directly are the effective molar concentrations $C_{+, \text{eff}}$ and $C_{-, \text{eff}}$.

4.2. Stochastic tug-of-war

The stochastic tug-of-war between the plus and minus motors can be described by an appropriate generalization of the model as given by Eq. (3.1) to the case of two motor species. The cargo particle now carries N_+ plus motors and N_- minus motors, and the cargo can attain $(N_+ + 1)(N_- + 1)$ states (n_+, n_-) which are characterized by the actual numbers n_+ and n_- of plus and minus motors that pull at the same time. These states form a square lattice as shown in Fig. 6.

When the cargo particle dwells in state (n_+, n_-) , it can undergo up to four different transitions. The unbinding of a plus motor from this state is governed by the rate

$$\omega(n_+, n_- | n_+ - 1, n_-) \equiv \omega_{\text{off},+}(n_+, n_-) = n_+ \kappa_{\text{off},+} e^{F_{1+}/F_{d,+}}, \quad (4.7)$$

the unbinding of a minus motor by the rate

$$\omega(n_+, n_- | n_+, n_- - 1) \equiv \omega_{\text{off},-}(n_+, n_-) = n_- \kappa_{\text{off},-} e^{|F_{1-}|/F_{d,-}}. \quad (4.8)$$

In addition, the binding rates of a plus and a minus motor are equal to

$$\omega(n_+, n_- | n_+ + 1, n_-) \equiv \omega_{\text{on},+}(n_+, n_-) = (N_+ - n_+) \omega_{\text{on},+} \quad (4.9)$$

and

$$\omega(n_+, n_- | n_+, n_- + 1) \equiv \omega_{\text{on},-}(n_+, n_-) = (N_- - n_-) \omega_{\text{on},-}. \quad (4.10)$$

So far, the two unbinding rates in Eqs. (4.7) and (4.8) have been expressed in terms of the two forces F_{1+} and F_{1-} experienced by a single plus and minus motor. It is important to note, however, that these two forces are not independent of each other, but are strongly coupled during cargo transport as soon as both motor species are active, i.e., as soon as both $n_+ > 0$ and $n_- > 0$. This can be understood from the force balance explained in the next subsection.

4.3. Force balance between two motor species

Thus, let us consider a cargo state (n_+, n_-) with $n_+ > 0$ and $n_- > 0$. The forces experienced by a single plus and a single minus motor are denoted by F_{1+} and F_{1-} as before. The total force experienced by the n_+ plus motors is then equal to

$$F_{n_+} = n_+ F_{1+} > 0. \quad (4.11)$$

Likewise, the total force experienced by the minus motors is

$$F_{n_-} = n_- F_{1-} < 0. \quad (4.12)$$

In the absence of an external load force, Newton's third law implies that⁴

$$F_{n_+} = |F_{n_-}| \quad \text{or} \quad n_- F_{1+} = n_+ |F_{1-}|. \quad (4.13)$$

For a given state (n_+, n_-) , one can distinguish three cases depending on the relative size of $n_+ F_{s,+}$ and $n_- F_{s,-}$. The first case with $n_+ F_{s,+} > n_- F_{s,-}$ corresponds to plus motor dominance. Likewise, the second case with $n_- F_{s,-} > n_+ F_{s,+}$ describes minus motor dominance. Both cases are smoothly connected by the special case with $n_- F_{s,-} = n_+ F_{s,+}$.

For *plus motor dominance* with $n_+ F_{s,+} > n_- F_{s,-}$, the plus motors step forward if a single plus motor experiences the load force $F_{1+} < F_{s,+}$ which implies that the n_+ plus motors feel the load $F_{n_+} = n_+ F_{1+} < n_+ F_{s,+}$. In addition, the minus motors step backward if a single minus motor experiences the load force $|F_{1-}| > F_{s,-}$ and the n_- minus motors feel the load $|F_{n_-}| = n_- |F_{1-}| > n_- F_{s,-}$. Because of the relation $F_{n_+} = |F_{n_-}|$ as given by Eq. (4.13), these two inequalities can be combined into

$$n_- F_{s,-} < F_{n_+} = |F_{n_-}| < n_+ F_{s,+}, \quad (4.14)$$

which is a necessary condition for forward steps of the plus motors and backward steps of the minus motors. For *minus motor dominance* with $n_- F_{s,-} > n_+ F_{s,+}$, the same kind of reasoning leads to the expression

$$n_+ F_{s,+} < F_{n_+} = |F_{n_-}| < n_- F_{s,-}, \quad (4.15)$$

which is a necessary condition for forward steps by the minus motors and backward steps of the plus motors. The two conditions (4.14) and (4.15) can now be combined into the general condition $\min(n_+ F_{s,+}, n_- F_{s,-}) \leq F_{n_+} = |F_{n_-}| \leq \max(n_+ F_{s,+}, n_- F_{s,-})$,

where the equalities include the special case with $n_+ F_{s,+} = n_- F_{s,-}$.

The two inequalities in Eq. (4.16) imply that the force F_{n_+} experienced by the n_+ plus motors can be expressed as

$$F_{n_+} = (1 - \lambda) n_- F_{s,-} + \lambda n_+ F_{s,+} \quad \text{with } 0 < \lambda < 1. \quad (4.17)$$

What remains to be done is to determine the parameter λ . This can be achieved by matching the instantaneous velocities of the plus and minus motors.

4.4. Matching of instantaneous velocities

When the cargo particle is in state (n_+, n_-) , its instantaneous velocity $v_{\text{ca}}(n_+, n_-)$ must be equal to the instantaneous velocities of both the plus motors and the minus motors, which implies $v_{\text{ca}}(n_+, n_-) = \mathcal{V}_+(F_{1+}) = \mathcal{V}_-(|F_{1-}|)$.

The second equality is equivalent to the implicit equation

$$\mathcal{V}_+(F_{n_+}/n_+) = \mathcal{V}_-(F_{n_-}/n_-) \quad (4.19)$$

for the force F_{n_+} where the force balance equation $|F_{n_-}| =$

⁴ In the presence of an external load force F_{ex} , the force balance becomes $F_{n_+} = |F_{n_-}| + F_{\text{ex}}$.

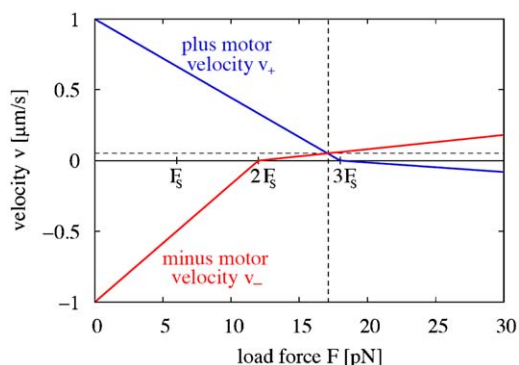


Fig. 7. Graphical solution of the matching condition (4.19) for the instantaneous cargo velocity $v = v_{ca}(n_+, n_-)$ and the total load force $F = F_{n_+}$, experienced by the n_+ plus motors in state $(n_+, n_-) = (3, 2)$ with $F_{n_+} = |F_{n_-}|$. Both the force-velocity relationship $v_+ = \mathcal{V}_+(F/n_+)$ for the plus motors (blue lines) and the corresponding relationship $v_- = \mathcal{V}_-(F/n_-)$ for the minus motors (red lines) have been taken to be piece-wise linear. The intersection point of these two functions determines the cargo velocity $v = v_{ca}(n_+, n_-)$ and the total load force $F = F_{n_+}$ as indicated by the broken lines. (For interpretation of the references to color in this figure legend, the reader is referred to the web version of this article.)

$n_-|F_{n_-}| = F_{n_+}$ has been used again. If F_{n_+} is expressed in terms of the parameter λ as in Eq. (4.17), the matching condition (4.19) becomes an implicit equation for this parameter.

The matching condition $\mathcal{V}_+(F_{n_+}/n_+) = \mathcal{V}_-(F_{n_+}/n_-)$ can be solved graphically. In order to do so, one has to plot the two rescaled force-velocity relationships $\mathcal{V}_+(F_{n_+}/n_+)$ and $\mathcal{V}_-(F_{n_+}/n_-)$ as a function of F_{n_+} . An example for such a graphical solution is shown in Fig. 7 for the cargo state $(n_+, n_-) = (3, 2)$ and for piece-wise linear force-velocity relationships. In the latter case, one may also obtain an explicit relation for the parameter λ , see Ref. [26].

In this way, one can determine the total load force $F_{n_+} = F_{n_+}(n_+, n_-)$ experienced by the n_+ plus motors for all cargo states (n_+, n_-) . The force F_{n_+} can then be used to calculate the forces $F_{1+} = F_{n_+}/n_+$ and $|F_{1-}| = F_{n_+}/n_-$ as experienced by a single plus and minus motor, respectively. When these expressions are inserted into the relations (4.7) and (4.8), one obtains the rate

$$\omega_{\text{off},+}(n_+, n_-) = n_+ \kappa_{\text{off},+} e^{F_{n_+}(n_+, n_-)/n_+ F_{d,+}} \quad (4.20)$$

for the unbinding of one plus motor from state (n_+, n_-) and the corresponding rate

$$\omega_{\text{off},-}(n_+, n_-) = n_- \kappa_{\text{off},-} e^{F_{n_+}(n_+, n_-)/n_- F_{d,-}} \quad (4.21)$$

for the unbinding of one minus motor. These two expressions show explicitly that these unbinding rates provide a direct coupling between the motor numbers n_+ and n_- .

4.5. Different motility states of cargo particles

The stochastic tug-of-war model described in the previous subsections leads to rather complex dynamic behavior related to seven different motility states. These motility states can be distinguished by the qualitative shape of the steady state distributions $P^{\text{st}}(n_+, n_-)$ for the two motor numbers n_+ and n_- . First, there are three different states for which the distribution $P^{\text{st}}(n_+, n_-)$ has a *single maximum*. This single maximum may be located at the boundaries of the (n_+, n_-) -plane with $(n_+, n_-) = (n_+, 0)$ or $(n_+, n_-) = (0, n_-)$, compare Fig. 6. These states represent fast plus directed or minus directed motion. Alternatively, this maximum may be located away from the boundaries of the (n_+, n_-) -plane and then corresponds to a ‘no motion’ state in which the two motor species block each other and the cargo

particle exhibits a strongly reduced cargo velocity as determined by the velocity of the backward stepping motors.

Second, the cargo can attain three different motility states for which the distribution $P^{\text{st}}(n_+, n_-)$ has *two local maxima*. Both of these maxima may be located at the boundaries of the (n_+, n_-) -plane and then lead to the switching between fast plus directed and fast minus directed motion, i.e., to bi-directional transport without pauses. In addition, the distribution $P^{\text{st}}(n_+, n_-)$ may have one maximum away from the boundary of the cargo’s state space and one maximum at this boundary. These latter distributions represent uni-directional transport in the plus or minus direction interrupted by prolonged pauses (or strongly reduced transport). Finally, the distribution $P^{\text{st}}(n_+, n_-)$ may exhibit *three local maxima* corresponding to bi-directional transport interrupted by pauses.

As one changes the single motor parameters and/or the motor numbers N_+ and N_- , the system may undergo a transition from one motility state to another. The most important single motor parameters that determine the cargo’s motility state are the two desorption coefficients

$$k_{\text{off},+} \equiv \frac{\kappa_{\text{off},+}}{\omega_{\text{on},+}} \quad \text{and} \quad k_{\text{off},-} \equiv \frac{\kappa_{\text{off},-}}{\omega_{\text{on},-}} \quad (4.22)$$

as well as the force ratios

$$f_+ \equiv \frac{F_{s,+}}{F_{d,+}}, \quad f_- \equiv \frac{F_{s,-}}{F_{d,-}} \quad \text{and} \quad f_s \equiv \frac{F_{s,+}}{F_{s,-}}. \quad (4.23)$$

4.6. Motility states for a symmetric tug-of-war

A particularly instructive case is provided by a ‘symmetric’ tug-of-war that is defined by the following two simplifying features: (i) equal numbers of plus and minus motors, i.e., $N_+ = N_-$ and (ii) identical single motor parameters for plus and minus motors apart from their preferred directions. This latter feature implies the equalities

$$k_{\text{off},+} = k_{\text{off},-} \equiv k_{\text{off}}, \quad f_+ = f_- \equiv f \quad \text{and} \quad f_s = 1 \quad (4.24)$$

for the desorption coefficients and force ratios and, thus, leads to a useful reduction in the number of parameters.

As one varies the force ratio f and the desorption coefficient k_{off} , the cargo particle exhibits three different motility states as shown in Fig. 8 for $N_+ = N_- = 4$: (i) ‘No motion’ states for small values of the force ratio f corresponding to weak motors. In these states, the motor number distribution $P^{\text{st}}(n_+, n_-)$ has a single maximum along the diagonal of the (n_+, n_-) -plane with $n_+ = n_-$ or $n_+ = n_- \pm 1$; (ii) bi-directional transport states *without* pauses for large values of f and desorption coefficients k_{off} that exceed a certain threshold value. The corresponding motor number distribution has two maxima of equal height at $(n_+, n_-) = (n_+, 0)$ and $(n_+, n_-) = (0, n_-)$. (iii) Bi-directional transport states *with* pauses for relatively large values of f and small values of k_{off} . In this latter case, the distribution $P^{\text{st}}(n_+, n_-)$ has three local maxima at $(n_+, n_-) = (n_+, 0)$, $(n_+, n_-) = (n', n')$, and $(n_+, n_-) = (0, n_-)$.

The different behavior of the three distinct motility regimes is illustrated in Fig. 9 for the three parameter values (f, k_{off}) corresponding to the crosses A, B, and C in Fig. 8. State A with $(f, k_{\text{off}}) = (2/3, 1/5)$ belongs to the ‘no motion’ regime, state B with $(f, k_{\text{off}}) = (6/3, 1/5)$ to the regime of bi-directional transport without pauses, and state C with $(f, k_{\text{off}}) = (4.75/3, 0.4/5)$ to the regime of bi-directional transport with pauses, see the three columns in Fig. 9. Each column contains the motor number distribution $P^{\text{st}}(n_+, n_-)$, a typical trajectory of the cargo particle, and the distribution of instantaneous cargo velocities.

As shown in the left column of Fig. 9, the distribution $P^{\text{st}}(n_+, n_-)$ for motility state A has a single maximum located at

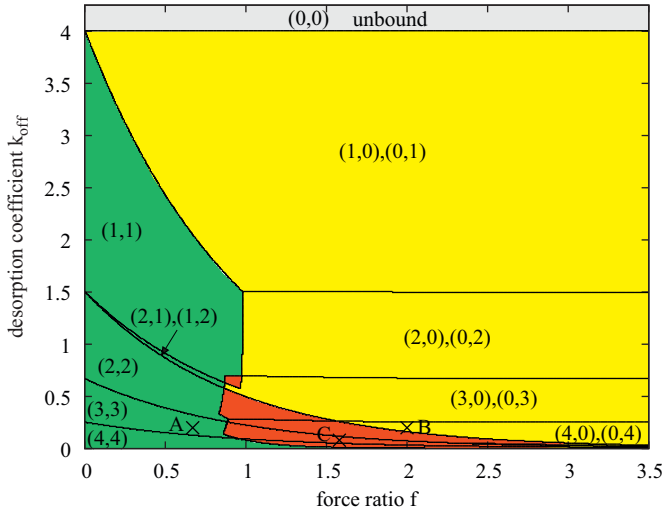


Fig. 8. Motility diagram for the symmetric tug-of-war of $N_+ = 4$ plus and $N_- = 4$ minus motors as a function of the force ratio f and the desorption coefficient k_{off} . Both motor species have identical single motor parameters apart from their preferred direction. Depending on the ratio $f = F_+/F_-$ of stall to detachment force and on the desorption coefficient $k_{\text{off}} = \kappa_{\text{off}}/\omega_{\text{on}}$, the cargo particle exhibits three different types of motility states: (i) ‘No motion’ states (green) for small values of the force ratio f . The motor number distribution $P^{\text{st}}(n_+, n_-)$ has a single maximum located at $(n_+, n_-) = (n, n)$ or $(n_+, n_-) = (n, n \pm 1)$. For sufficiently small values of the desorption coefficient k_{off} , the number n attains its maximal value $n = 4$ and decreases monotonically with increasing k_{off} ; (ii) bi-directional transport states without pauses (yellow) for large values of f and desorption coefficients k_{off} that exceed a certain threshold. The corresponding distribution $P^{\text{st}}(n_+, n_-)$ has two maxima located at $(n_+, n_-) = (n, 0)$ and $(n_+, n_-) = (0, n)$; and (iii) bi-directional transport states with pauses (red) for large f and small k_{off} . The three states labeled by A, B, and C are described in more detail in Fig. 9 [26]. (For interpretation of the references to color in this figure legend, the reader is referred to the web version of this article.)

$(n_+, n_-) = (3, 3)$. This state exhibits no motion of the cargo apart from small fluctuations in both directions, and an instantaneous velocity distribution with a single peak at zero cargo velocity. In contrast, state B has a motor number distribution with two maxima at $(n_+, n_-) = (4, 0)$ and $(n_+, n_-) = (0, 4)$. In this state, the cargo performs fast directed motion both in the plus and in the minus direction but this motion does not exhibit any pauses. The latter property also follows from the velocity distribution, which is bimodal with two peaks of equal height at $v_{\text{ca}} = \pm 1 \mu\text{m/s}$. Finally, state C is characterized by a motor number distribution with three maxima at $(n_+, n_-) = (4, 0)$, $(n_+, n_-) = (3, 3)$, and $(n_+, n_-) = (0, 4)$. The cargo trajectories now exhibit fast motion in both directions as well as prolonged pauses leading to a velocity distribution with three peaks.

As one varies the motor numbers N_+ and N_- with $N_+ = N_- = N_1$, the qualitative features of the motility diagram and of the corresponding motility states of the cargo as illustrated in Figs. 8 and 9 for $N_1 = 4$ remain unchanged as has been shown by explicit simulations for $2 \leq N_1 \leq 10$ [27].⁵ As the motor number N_1 is increased, the distributions $P^{\text{st}}(n_+, n_-)$ exhibit sharper and sharper maxima, and the switching times between these maxima increase exponentially with N_1 [53] as has been numerically studied up to $N_1 = 80$. This implies that the tug-of-war system leads to nonequilibrium phase transitions in the limit of large N_1 .

⁵ The case $N_1 = 1$ is special since it does not exhibit any states corresponding to the regime of bi-directional transport with pauses.

5. Traffic of motors and cargo particles

In this final section, we briefly review traffic phenomena that arise when many motors and/or cargo particles are bound to the filaments and the bound motors and particles start to bump into each other. Depending on their interactions and on the compartment geometry, the motors can then form various spatio-temporal patterns such as traffic jams and undergo nonequilibrium phase transitions between different transport patterns.

5.1. Dilute transport regime

First, it is useful to give a precise definition of the dilute transport regime, in which the bound motors and cargos can be treated as noninteracting particles. This definition will involve several molecular length scales including the lattice constant ℓ of the filament. For microtubules, this lattice constant is equal to the step size of the kinesin and dynein motors. In general, a single motor without a cargo particle covers or occupies ℓ_{mo}/ℓ binding sites of the filament. The ratio ℓ_{mo}/ℓ should typically assume a value between $\ell_{\text{mo}}/\ell = 1$ for single-site occupancy and $\ell_{\text{mo}}/\ell = 2$ for two-site occupancy [6]. In all cases, the ratio ℓ_{mo}/ℓ should be of order one.

If many motors are bound to the filaments and the system is characterized by binding ratio n_b , see Eq. (2.9), the probability ρ_b that a single binding site is occupied by a motor is given by

$$\rho_b = (\ell_{\text{mo}}/\ell)n_b \approx \ell_{\text{mo}}C/\ell C_{\text{dis}}, \quad (5.1)$$

with the dissociation constant C_{dis} as defined by Eq. (2.10). The probability that the motor can reach the next binding site in the forward direction is then $(1 - \rho_b)$ which is also equal to the probability that the motor can make a forward step without bumping into another bound motor. Therefore, the probability that the motor can make $\langle \Delta x \rangle / \ell$ successive steps without interactions with other bound motors is given by $(1 - \rho_b)^{\langle \Delta x \rangle / \ell} \approx \exp[-\langle \Delta x \rangle \rho_b / \ell]$. The dilute transport regime is defined by the criterion that this latter probability is close to one which implies the inequality

$$\rho_b \ll \ell / \langle \Delta x \rangle \quad (5.2)$$

for the single-site occupation probability ρ_b . It then follows from Eq. (5.1) that the molar concentration C of the motors should belong to the concentration regime defined by

$$C \ll C_* \equiv \frac{\ell}{\ell_{\text{mo}}} \frac{\ell}{\langle \Delta x \rangle} C_{\text{dis}}. \quad (5.3)$$

For kinesin motors on microtubules with lattice constant (and step size) $\ell = 8 \text{ nm}$, average run length $\langle \Delta x \rangle = 1 \mu\text{m}$, and dissociation constant $C_{\text{dis}} = 100 \text{ nM}$, the crossover concentration $C_* \approx 1 \text{ nM}$ which represents a rather small concentration.

Alternatively, we may consider the average separation $\langle L_{b,b} \rangle = \ell / n_b$ of the bound motors. The inequality (5.2) then implies that the dilute transport regime corresponds to $\langle L_{b,b} \rangle \gg (\ell_{\text{mo}}/\ell) \langle \Delta x \rangle$.

Since the ratio $\ell_{\text{mo}}/\ell \geq 1$, the dilute transport regime for a single motor without cargo is also defined by the criterion that the average separation $\langle L_{b,b} \rangle$ of the bound motors is large compared to their run length $\langle \Delta x \rangle$.

This line of arguments can be easily generalized to the situation of cargo particles pulled by single motors. In this case, the relation (2.10) still applies provided C , C_{dis} , and n_b now denote the molar concentration, dissociation constant, and binding ratio of the cargo particles. If these cargo particles cover ℓ_{ca}/ℓ binding sites of the filament with $\ell_{\text{ca}}/\ell > \ell_{\text{mo}}/\ell$, the single site occupation probability ρ_b is now given by $\rho_b = (\ell_{\text{ca}}/\ell)n_b$. It then follows from

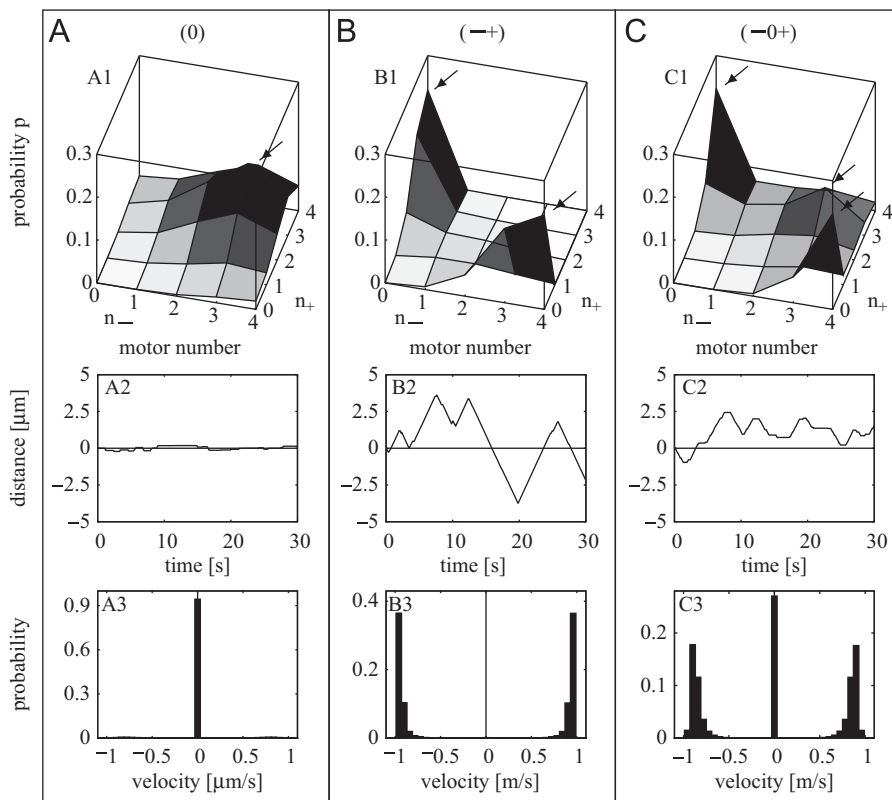


Fig. 9. Three motility states A, B, and C of a symmetric tug-of-war between $N_+ = 4$ plus and $N_- = 4$ minus motors corresponding to the three crosses in the motility diagram of Fig. 8: (A) ‘No motion’ state: (A1) motor number distribution $P^{st}(n_+, n_-)$ with a single maximum at $(n_+, n_-) = (3, 3)$; (A2) typical cargo trajectory with small excursions around the start position; and (A3) distribution of instantaneous cargo velocities with a single peak at zero velocity. (B) *Bi-directional transport state without pauses*: (B1) motor number distribution with two maxima at $(n_+, n_-) = (4, 0)$ and $(n_+, n_-) = (0, 4)$; (B2) typical cargo trajectory with fast directed motion both in the plus and in the minus direction; and (B3) velocity distribution with two peaks at cargo velocities $v_{ca} = \pm 1 \mu\text{m/s}$. (C) *Bi-directional transport state with pauses*: (C1) motor number distribution with three maxima at $(n_+, n_-) = (4, 0)$, $(n_+, n_-) = (3, 3)$, and $(n_+, n_-) = (0, 4)$; (C2) typical cargo trajectory with fast directed motion both in the plus and in the minus direction interrupted by prolonged pauses; and (C3) distribution of instantaneous cargo velocity with three peaks [26].

the inequality (5.2) for ρ_b that the dilute transport regime of cargo particles pulled by a single motor corresponds to the regime

$$C \ll C_{**} \equiv \frac{\ell}{\ell_{ca}} \frac{\ell}{\langle \Delta x \rangle} C_{dis} \quad (5.5)$$

for the molar concentration of these cargo particles. The cargo size ℓ_{ca} can be much larger than the lattice constant (or step size) ℓ which implies that the crossover concentration C_{**} , which defined the dilute transport regime, can be strongly reduced by the factor ℓ/ℓ_{ca} . The expression (5.5) for C_{**} , which involves the lateral size ℓ_{ca} of the cargo particles, will also approximately apply to the more general case of cargo particles pulled by N motors as long as the average step size of these cargo particles is of the order of ℓ .

5.2. Overcrowding of filaments and traffic jams

For motor concentrations C that exceed the crossover concentration C_{**} , the bound motors start to interact with each other, and these interactions become particularly strong when the filaments become overcrowded for concentrations $C \gtrsim C_{dis}$ as follows from the definition (2.10) of the dissociation constant.

From the theoretical point of view, the overcrowding of filaments by motors should lead to traffic jams. These jams are particularly pronounced in tube-like compartments that represent primitive models of axons [12,29–31]. Because of such traffic jams, the current or flux of the bound motors exhibits a maximum as one increases the total number of motors in the system. For a long tube-like compartment, e.g., the maximum is reached for half

filling of the filament sites corresponding to binding ratio $n_b = 1/2$ [29]. The half filling condition applies to simple motor walks, for which one ignores the details of the chemomechanical motor cycles, provided the motors occupy a single filament site and $z \equiv \ell_{mo}/\ell = 1$. If the motors occupy $z > 1$ binding sites, the maximum current is already reached for binding ratios $n_b = 1/(z + \sqrt{z}) < 1/2$. On the other hand, if the motors occupy a single site but can dwell in two internal states, the maximum current is reached for binding ratios $n_b > 1/2$ as shown in Ref. [54].

It is remarkable that the largest binding ratio reached by the kinesins as studied experimentally in Ref. [39], is about $n_b = 1/2$. This seems to imply that these kinesin motors are able to avoid traffic jams in some way. As previously discussed in Ref. [6], several possible mechanisms for such a behavior can be envisaged: (i) the lateral size of stepping kinesins is increased compared to static kinesins; (ii) stepping kinesins could increase their unbinding rate by bumping into each other; (iii) stepping kinesins could reduce the binding rate for kinesin from the bulk solution, e.g., because of hydrodynamic interactions. Such a mechanism would imply that the effective binding rate decreases with increasing motor velocity; and (iv) the motors experience mutual interactions that lead to a certain preferred separation of the stepping kinesins. Further experiments seem to be necessary in order to clarify this issue. Jams of molecular motors have also been observed for other in vitro systems as described in Refs. [36–38].

Traffic jams are also expected to occur for the traffic of cargo particles. If the cargo particles are pulled by a single motor species, the cargo traffic is expected to be rather similar to the

traffic of single motor molecules. For cargo particles pulled by two antagonistic motor teams, on the other hand, one would intuitively expect that jams can be reduced by bi-directional transport. Indeed, if a jam builds up in one direction, e.g., because of an obstacle, the cargo particles at the very end of the jam may then start to move in the opposite direction and, in this way, to dissolve the jam. This effect can be studied in more detail if one maps the bi-directional motion of many cargo particles onto lattice walks with both forward and backward steps.

5.3. Nonequilibrium phase transitions in motor traffic

In our previous studies of motor traffic, we encountered several examples of nonequilibrium phase transitions [29,40,30]. Such transitions are interesting because a small change in a parameter leads to a huge response of the motor system and its transport properties.

The first examples for phase transitions in motor traffic were theoretically found for tube-like compartments with open orifices [29]. These transitions occur as one changes the boundary densities at these two orifices and are intimately related to the phase transitions found for asymmetric simple exclusion processes (ASEPs) in one dimension. The latter processes have been studied for a variety of systems, see, e.g., Refs. [55–61]; an extensive review of ASEPs is contained in Ref. [62]. In the last couple of years, several groups have also studied one-dimensional ASEPs in contact with particle reservoirs [63–65], which are closely related to the tube-like systems introduced in Refs. [12,29].

A special kind of phase transition occurs in a half-open tube as shown in Fig. 10(a) [30]. The left orifice is open, the right orifice is closed, a geometry that resembles the geometry of an axon. The closed orifice corresponds to the synaptic terminal whereas the motor reservoir at the open orifice corresponds to the cell body, where the motors are synthesized. Let us focus on the situation in which the tube contains only minus motors that would correspond to dynein motors in axons. The minus motors enter the tube by diffusing through the left orifice. Once they are bound to the filament, they walk back towards this orifice. As a result of this competition, the minus motors penetrate only up to a finite distance from the left orifice. As one decreases the velocity, e.g., by decreasing the ATP concentration and, thus, the chemical energy input $\Delta\mu$, this penetration increases and the minus motors form a traffic jam along the filament in front of the left orifice. This jam length diverges as $1/v$ for small v [30]. In these two examples of traffic phase transitions, the only interaction between the motors is provided by their mutual exclusion.

Another type of transition, that can be explored by varying the motor concentrations, occurs in systems with two species of motors that walk in opposite directions [40]. The simplest geometry is again provided by a tube-like compartment with

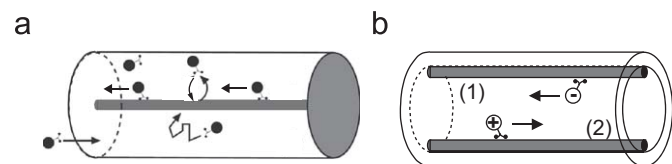


Fig. 10. Tube-like compartments that lead to nonequilibrium phase transitions in motor traffic: (a) half-open tube with one motor species. When bound to the filament, the motors move towards the open orifice on the left. For small motor velocity, a jam builds up in front of this orifice. The jam length diverges in the limit of vanishing velocity or vanishing ATP concentration [30] and (b) tube with two motor species that walk into opposite directions and compete for the same binding sites on the filaments. This system undergoes a symmetry breaking phase transition, at which each filament becomes covered by either plus or minus motors [40].

periodic boundary conditions as shown in Fig. 10(b). Alternatively, one may consider systems with a constant density of unbound motors. As long as the motor–motor interactions are purely repulsive, the flux of bound motors is determined by the majority species, and the system evolves smoothly as one varies the motor concentrations. The situation becomes more interesting if one includes another, effectively attractive interaction between the bound motors as suggested by decoration experiments [66–69] in which filaments are decorated by motors and bare filament segments are observed to coexist with highly decorated segments. If the strength of this interaction is described by the parameter q , the system undergoes a traffic phase transition at a critical value $q = q_c$ [40]. This phase transition occurs between two states with a spontaneously broken symmetry, for which one motor species is essentially excluded from the filaments. As one varies the bulk composition of the motors, the total motor flux develops a hysteresis loop across the phase boundary. In addition, if the system contains groups of isopolar filaments, the broken symmetry is directly visible via the coexistence of traffic lanes with opposite directionality as indicated in Fig. 10(b).

6. Summary and outlook

In this article, we have reviewed recent studies on the cooperative behavior of molecular motors related to cargo transport and traffic phenomena. The theoretical description of this behavior is based on the properties of single motor molecules as briefly reviewed in Section 2. Cooperative transport by teams of molecular motors can lead to fast uni-directional or bi-directional motion as described in Sections 3 and 4, respectively. In addition, pattern formation processes and phase transitions in motor traffic have been briefly discussed in Section 5.

A single team of identical motors leads to uni-directional cargo transport as described in Section 3. This cooperative transport mode has several advantages. First, the run length of the cargo particle is strongly increased with increasing motor number, see the explicit expression (3.9) and the comparison between theory and experiment in Fig. 4 [15,17]. Second, compared to a single motor, a team of N motors can generate larger forces. This follows from the explicit expression (3.27) for the average cargo velocity in the presence of a load force. If a single motor has stall force F_s , the team of N identical motors has an apparent stall force that is of the order of NF_s for relatively small N but substantially smaller than NF_s for large N [15]. Third, cooperative transport by N motors offers additional possibilities for regulation. One example is provided by binding defects of the filaments such as tau proteins that reduce the rebinding rate of the detached motors [15,70].

In eukaryotic cells, vesicles and other cargo particles often carry both kinesins and dyneins, which leads to bi-directional transport along microtubules. The observed transport behavior can be understood in terms of a stochastic tug-of-war between the two motor teams as explained in Section 4 [26,27]. In order to define such a tug-of-war in a consistent manner, one has to take the instantaneous force balance between the two motor teams into account, see Section 4.3, which enters the transition rates between the different cargo states, see Section 4.4. The stochastic tug-of-war leads to rather complex transport behavior as observed experimentally. In general, one finds seven distinct motility regimes, which can be distinguished by the qualitative features of the motor number distribution $P^{\text{st}}(n_+, n_-)$ as explained in Section 4.5. A particularly simple case is provided by a symmetric tug-of-war, see Section 4.6, because the symmetry reduces the number of possible motility states from seven to three. The corresponding motility diagram is shown in Fig. 8 and the motility

behavior for the different regimes is illustrated in Fig. 9. The general, asymmetric case is considered in Refs. [26,27].

The molecular motors considered here are found in all eukaryotic cells and provide the main machinery for force production and cargo transport in biological systems [71]. On the one hand, we would like to obtain a systematic understanding of these biological processes. On the other hand, such an understanding is also necessary in order to construct useful biomimetic systems that are based on molecular motors. One example is provided by biomimetic transport systems that are inspired by the transport in axons since such systems represent promising alternatives to microfluidic devices, in which transport is coupled to flow induced by external pressure. Compared to pressure-induced flow, the transport by motors has several advantages such as: (i) cargo transport is hardly affected by the viscosity of the aqueous solution and, thus, remains efficient even in a dense solution of macromolecules; (ii) using two different motor species, different types of cargo can be simultaneously transported in both directions; and (iii) this transport system does not require rigid compartment walls but works in soft and flexible compartments as well. Another application of motors is their active diffusion, by which one can increase the diffusion constant of micrometer-sized cargo particles by several orders of magnitude [14]. When integrated into existing biochips for DNA and RNA hybridization, these transport systems would act to increase the hybridization rates.

In general, active biomimetic systems based on molecular motors and filaments should have many applications in bioengineering, pharmacology and medicine. Such applications include sorting devices for biomolecules, motile drug delivery systems, molecular shuttles in 'labs-on-a-chip', and switchable scaffolds for tissue engineering. Thus, molecular motors and filaments are likely to become key components in the emerging soft nanotechnology.

Acknowledgments

This review is based on the final report for STREP Project no. NMP4-CT-2004-516989 within the EC Sixth Framework Program.

References

- [1] D. Bray, *Cell Movements*, Garland Publishing, New York, 2001.
- [2] J. Howard, *Mechanics of Motor Proteins and the Cytoskeleton*, first ed., Sinauer, New York, 2001.
- [3] M. Schliwa, G. Woehlke, *Nature* 422 (2003) 759.
- [4] R.D. Vale, *Cell* 112 (2003) 467.
- [5] R. Lipowsky, S. Klumpp, *Physica A* 352 (2005) 53.
- [6] R. Lipowsky, Y. Chai, S. Klumpp, S. Liepelt, M.J.I. Müller, *Physica A* 372 (2006) 34.
- [7] R. Lipowsky, S. Liepelt, A. Valleriani, *J. Stat. Phys.*, 135 (2009) 951.
- [8] K. Svoboda, Ch.F. Schmidt, B.J. Schnapp, St.M. Block, *Nature* 365 (1993) 721.
- [9] A. Yildiz, M. Tomishige, R.D. Vale, P.R. Selvin, *Science* 303 (2004) 676.
- [10] N.J. Carter, R.A. Cross, *Nature* 435 (2005) 308.
- [11] S.M. Block, L.S.B. Goldstein, B.J. Schnapp, *Nature* 348 (1990) 348.
- [12] R. Lipowsky, S. Klumpp, T.M. Nieuwenhuizen, *Phys. Rev. Lett.* 87 (2001) 108101.
- [13] T.M. Nieuwenhuizen, S. Klumpp, R. Lipowsky, *Europhys. Lett.* 58 (2002) 468.
- [14] S. Klumpp, R. Lipowsky, *Phys. Rev. Lett.* 95 (2005) 268102.
- [15] S. Klumpp, R. Lipowsky, *Proc. Nat. Acad. Sci. USA* 102 (2005) 17284.
- [16] M. Vershiniin, B.C. Carter, D.S. Razafsky, S.J. King, S.P. Gross, *Proc. Nat. Acad. Sci. USA* 104 (2007) 87.
- [17] J. Beeg, S. Klumpp, R. Dimova, R.S. Gracia, E. Unger, R. Lipowsky, *Biophys. J.* 94 (2008) 532.
- [18] R.H. Miller, R.J. Lasek, *J. Cell Biol.* 101 (1985) 2181.
- [19] A. Ashkin, K. Schütze, J.M. Dziedzic, U. Euteneuer, M. Schliwa, *Nature* 348 (1990) 346.
- [20] S.P. Gross, M.A. Welte, S.M. Block, E.F. Wieschaus, *J. Cell Biol.* 156 (2002) 715.
- [21] D.B. Hill, M.J. Plaza, K. Bonin, G. Holzwarth, *Eur. Biophys. J.* 33 (2004) 623.
- [22] C. Kural, H. Kim, S. Syed, G. Goshima, V.I. Gelfand, P.R. Selvin, *Science* 308 (2005) 1469.
- [23] V. Levi, A.S. Serpinskaya, E. Gratton, V. Gelfand, *Biophys. J.* 90 (2006) 318.
- [24] S.P. Gross, *Phys. Biol.* 1 (2004) R1.
- [25] M.A. Welte, *Curr. Biol.* 14 (2004) R525.
- [26] M.J.I. Müller, S. Klumpp, R. Lipowsky, *Proc. Nat. Acad. Sci. USA* 105 (2008) 4609.
- [27] M.J.I. Müller, S. Klumpp, R. Lipowsky, *J. Stat. Phys.* 133 (2008) 1059.
- [28] M.A. Welte, S.P. Gross, *HFSP J.* 2 (2008) 178.
- [29] S. Klumpp, R. Lipowsky, *J. Stat. Phys.* 113 (2003) 233.
- [30] M.J.I. Müller, S. Klumpp, R. Lipowsky, *J. Phys. Cond. Mat.* 17 (2005) S3839.
- [31] S. Klumpp, M.J.I. Müller, R. Lipowsky, *Traffic of molecular motors*, in: A. Schadschneider, T. Pöschel, R. Kühne, M. Schreckenberg, D.E. Wolf (Eds.), *Traffic and Granular Flow '05*, Springer, Berlin, 2007, pp. 251–261.
- [32] D.D. Hurd, W.M. Saxton, *Genetics* 144 (1996) 1075.
- [33] M.A. Martin, S.J. Iyadurai, A. Gassman Jr., J.G. Gindhart, T.S. Hays, W.M. Saxton, *Mol. Biol. Cell* 10 (1999) 3717.
- [34] S. Konzack, *Funktion des Kinesin Motorproteins KipA bei der Organisation des Mikrotubuli-Cytoskeletts und beim polaren Wachstum von Aspergillus nidulans*, Doctoral Thesis, University of Marburg, 2004.
- [35] S. Konzack, P.E. Rischitor, C. Enke, R. Fischer, *Mol. Biol. Cell* 16 (2005) 497.
- [36] I.M.-T.C. Crevel, M. Nyitrai, M.C. Alonso, S. Weiss, M.A. Gevees, R.A. Cross, *EMBO J.* 23 (2004) 23.
- [37] C. Leduc, O. Campas, K.B. Zeldovich, A. Roux, P. Jolimaître, L. Bourel-Bonnet, B. Goud, J.-F. Joanny, P. Bassereau, J. Prost, *Proc. Nat. Acad. Sci. USA* 101 (2004) 17096.
- [38] K. Nishinari, Y. Okada, A. Schadschneider, D. Chowdhury, *Phys. Rev. Lett.* 95 (2005) 118101.
- [39] A. Seitz, T. Surrey, *EMBO J.* 25 (2006) 267.
- [40] S. Klumpp, R. Lipowsky, *Europhys. Lett.* 66 (2004) 90.
- [41] P. Kraikivski, R. Lipowsky, *J. Kierfeld, Phys. Rev. Lett.* 96 (2006) 258103.
- [42] J. Kierfeld, P. Gutjahr, T. Kühne, P. Kraikivski, R. Lipowsky, *J. Comp. Theor. Nanosci.* 3 (2006) 898.
- [43] S. Liepelt, R. Lipowsky, *Phys. Rev. Lett.* 98 (2007) 258102.
- [44] R. Lipowsky, S. Liepelt, *J. Stat. Phys.* 130 (2008) 39.
- [45] S. Liepelt, R. Lipowsky, *Phys. Rev. E* 79 (2009) 011917.
- [46] K. Visscher, M.J. Schnitzer, S.M. Block, *Nature* 400 (1999) 184.
- [47] M. Nishiyama, H. Higuchi, T. Yanagida, *Nat. Cell Biol.* 4 (2002) 790.
- [48] St.J. King, T.A. Schroer, *Nat. Cell Biol.* (2000) 20.
- [49] A.D. Mehta, R.S. Rock, M. Rief, J.A. Spudich, M.S. Mooseker, R.E. Cheney, *Nature* 400 (1999) 590.
- [50] Z. Ökten, L.S. Churchman, R.S. Rock, J.A. Spudich, *Nat. Struct. Mol. Biol.* 11 (2004) 884.
- [51] H.A. Kramers, *Physica VII* 4 (1940) 284.
- [52] M.J. Schnitzer, K. Visscher, S.M. Block, *Nat. Cell Biol.* 2 (2000) 718.
- [53] M.J.I. Müller, S. Klumpp, R. Lipowsky, in preparation.
- [54] S. Klumpp, Y. Chai, R. Lipowsky, *Phys. Rev. E* 78 (2008) 041909.
- [55] C.T. MacDonald, J.H. Gibbs, A.C. Pipkin, *Biopolymers* 6 (1968) 1.
- [56] F. Spitzer, *Adv. Math.* 5 (1970) 246.
- [57] S. Katz, J.L. Lebowitz, H. Spohn, *J. Stat. Phys.* 34 (1984) 497.
- [58] J. Krug, *Phys. Rev. Lett.* 67 (1991) 1882.
- [59] A.B. Kolomeisky, G.M. Schütz, E.B. Kolomeisky, J.P. Straley, *J. Phys. A Math. Gen.* 31 (1998) 6911.
- [60] J.L. Lebowitz, H. Spohn, *J. Stat. Phys.* 95 (1999) 333.
- [61] R.K.P. Zia, L.B. Shaw, B. Schmittmann, R.J. Aastalos, *Comput. Phys. Commun.* 127 (2000) 23.
- [62] G.M. Schütz, *Exactly solvable models for many-body systems far from equilibrium*, in: C. Domb, J.L. Lebowitz (Eds.), *Phase Transitions and Critical Phenomena*, vol. 19, Academic Press, London, 2001, pp. 3–251.
- [63] A. Parmeggiani, T. Franosch, E. Frey, *Phys. Rev. Lett.* 90 (2003) 086601.
- [64] V. Popkov, A. Rakoš, R.D. Willmann, A.B. Kolomeisky, G.M. Schütz, *Phys. Rev. E* 67 (2003) 066117.
- [65] M.R. Evans, R. Juhasz, L. Santen, *Phys. Rev. E* 68 (2003) 026117.
- [66] D.T. Woodrum, S.A. Rich, T.D. Pollard, *J. Cell Biol.* 67 (1975) 231.
- [67] A. Orlova, E.H. Egelman, *J. Mol. Biol.* 265 (1997) 469.
- [68] A. Vilfan, E. Frey, F. Schwabl, M. Thormählen, Y.-H. Song, E. Mandelkow, *J. Mol. Biol.* 312 (2001) 1011.
- [69] E. Muto, H. Sakai, K. Kaseda, *J. Cell Biol.* 168 (2005) 691.
- [70] Y. Chai, R. Lipowsky, S. Klumpp, *J. Stat. Phys.* 135 (2009) 241.
- [71] R. Lipowsky, A. Valleriani (Eds.), *Biophys. Rev. Lett.* 4 (2009) 1 (Special Issue).